International Journal of Power Electronics and Drive System (IJPEDS)
Vol. 9, No. 1, March 2018, pp. 286~296
ISSN: 2088-8694, DOI: 10.11591/ijpeds.v9.i1.pp286-296

Design of a Battery-Ultracapacitor Hybrid Energy-Storage System with Power Flow Control for an Electric Vehicle

B. K. Tan[1], N. M. L. Tan[2], A. K. Ramasamy[3]
[1]Squire Mech Sdn. Bhd., Subang Jaya, Malaysia
[2]Department of Electrical Power Engineering, Universiti Tenaga Nasional, Kajang, Malaysia
[3]Department of Electronics and Communications Engineering, Universiti Tenaga Nasional, Kajang, Malaysia

Article Info

Article history:

Received Nov 20, 2017
Revised Dec 10, 2017
Accepted Jan 11, 2018

Keyword:

Battery
Bidirectional isolated dc-dc converter
Hybrid energy storage
Multiple-input
Ultracapacitor

ABSTRACT

A combination of battery and ultracapacitor as a hybrid energy storage system (HESS) for an electric vehicle (EV) can result in better acceleration performance, reduced battery charge-discharge cycle and longer driving range. This paper presents a new converter design combining triple-half-bridge (THB) and boost half-bridge (BHB) converters in a battery-ultracapacitor HESS. The BHB converter is used to compensate the voltage variation of the ultracapacitor. A power management system is proposed to control the power of battery and ultracapacitor, to supply the demanded power of an EV. This paper describes the operation of the proposed converter using a simplified Δ-type primary-referred equivalent circuit. This paper also shows the simulation results verifying the fast dynamic response of the proposed power management system for the proposed HESS, with minimal current stress.

Corresponding Author:

N. M. L. Tan,
Department of Electrical Power Engineering,
Universiti Tenaga Nasional,
KM 7, Jalan IKRAM-Uniten, 43000 Kajang, Selangor, Malaysia.
Email: nadia@uniten.edu.my

1. INTRODUCTION

The design of the energy storage system in an EV should satisfy the demands of high power density for meeting the acceleration requirement, and of high energy density to attain the desired vehicle driving range. Typical energy storage devices for automotive applications are lead-acid, nickel metal hydride (NiMH), and lithium ion (Li-ion) batteries. The NiMH batteries dominate the EV market due to their lower cost as compared to the Li-ion batteries [1] and [2]. However, the characteristics of a Li-ion battery such as high monomer voltage and high energy density have become the preferred battery technology for EV [3]. The ultracapacitor is an energy storage device that have higher power density, faster charging and discharging rates, and longer cycle life than the batteries, complementing the characteristics of a Li-ion battery. Since, an ultracapacitor has low energy density, it is not suitable as the only energy storage device in an electric vehicle.

One of the drawbacks of the lithium ion battery is that it is not suitable for supplying a large amount of power in a short duration due to the limitation in its discharging capability. Moreover, frequent battery charging-discharging operations results in its lifetime reduction. Therefore, employing the ultracapacitor in a HESS for EV can improve the battery lifetime. The high power density characteristic of an ultracapacitor is able to meet peak power demand during EV acceleration and absorb regenerative braking power as the ultracapacitor is suitable for pulse-power operations. On the other hand, the lithium ion battery is suitable for operations that require high energy density.

In an EV operation, power output of the battery and ultracapacitor are variable and depends on the power demand. Moreover, the terminal voltage of an ultracapacitor varies widely during charging and discharging operations. Therefore, it is important for conversion system of the HESS to be capable of efficiently transferring power from two different energy storage devices in a wide input voltage range. Non-isolated and isolated multiple input dc-dc converters are often employed in HESS [4] - [6]. The multiple input dc-dc converter design for battery-ultracapacitor HESS employs power switching devices and diodes in the bidirectional dc-dc converters to control the power flow between the on-board energy storage devices and load [4] and [7]. However, it does not provide galvanic isolation for all power ports. Some applications require galvanic isolation for voltage matching and system safety. Hence, multiple-input bidirectional isolated dc-dc converters will be suitable for energy storage systems that combine various sources.

Figure 1 shows a current-source half-bridge bidirectional isolated dc-dc converter [6], [8-9]. The converter employs half the number of devices of the full bridge dc-dc converter at the same power rating without additional total device rating. Moreover, the converter achieves soft-switching in a wide operating range, requires less control, and limits current ripple, increasing battery lifetime. Nevertheless, there is a high current stress on the dc-dc converter when it is operated in a wide operating voltage range because the dc bus voltage ratio cannot match to the transformer turns ratio. Although, the PWM-plus-phase-shift (PPS) control strategy is proposed to minimize device current stress, the current stress problem at the low-voltage side of the dc-dc converter still persists [10] and [11].

Figure 2 presents a converter topology that combines voltage-source half-bridge bidirectional isolated dc-dc converter with a BHB converter [12]. This topology of dc-dc converter is suitable for applications in a wide operating voltage range, as it is able to minimize device current stress and solve asymmetric current stress problem by maintaining the dc voltage of V_{Hdc1} at the low-voltage side

An isolated multiport dc-dc converter for fuel cell-ultracapacitor HESS was presented in [13]. The terminal voltage of an ultracapacitor can vary between 50% and 100%, causing high current stress in the converter. The proposed converter utilizes PPS control to maintain a constant voltage across the half-bridge converter, minimizing the current stress.

This paper proposes a multiple-input dc-dc converter that can be employed for a battery-ultracapacitor HESS in an EV, which will be referred to as "the proposed HESS" from this point onwards. The proposed HESS topology combines the two converter topologies in Figures 1 and 2 with a three-winding high-frequency transformer. The bidirectional power flow is controlled using a simple phase-shift modulation. In addition, this paper describes the operating principles of the multiple-input dc-dc converter of the proposed HESS, discussing in detail the discharging mode of operation of both the battery and ultracapacitor. It also presents the circuit design and power flow control strategy employed. Finally, this paper shows the simulation results that verify the feasibility of the proposed HESS for EV application.

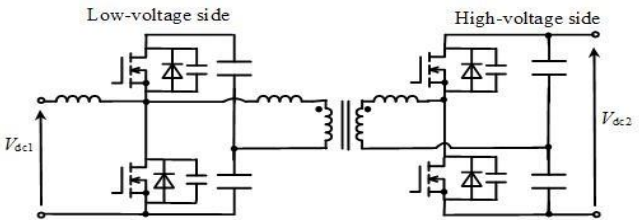

Figure. 1. Current-source half-bridge bidirectional isolated dc-dc converter [6].

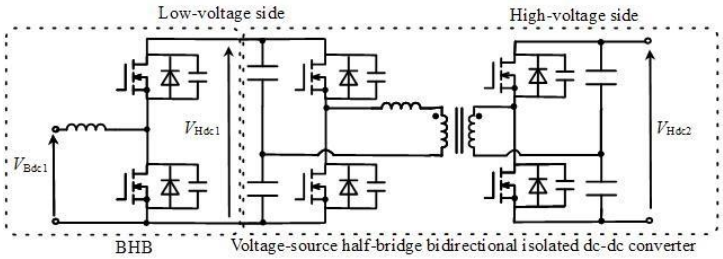

Figure 2. Voltage-source half-bridge bidirectional isolated dc-dc converter combined with a boost half-bridge (BHB) converter [12].

2. THE PROPOSED HESS AND OPERATING PRINCIPLES

Figure 3 presents the proposed HESS that consists of a multiple-input triple-half-bridge (THB) dc-dc converter combined with a BHB. The rated power of PHB_1 (proposed half bridge 1) is 6 kW, BHB (boost half bridge) and PHB_2 (proposed half bridge 2) is 8 kW, and PHB_3 is 12 kW. The dc bus of converters PHB_1 and PHB_3 (proposed half bridge 2) are connected to the battery and dc-load, respectively. Moreover, the BHB is combined with PHB_2 and the dc bus of the BHB is connected to the ultracapacitor. The converter PHB1 for the battery is selected as the device number of this topology is low and able to minimize ripple currents. The voltage at the battery side is V_{BT}, and at the high-voltage side it is V_{HV}. Since the voltage of the ultracapacitor V_{UC}, varies in a wide range and can cause high current stress in the proposed HESS, the BHB acts as a voltage regulator to keep the dc-link voltage of PHB_2, V_{Pdc2}, constant at the desired voltage and matched to the transformer turn ratio n_2 (N_{p2}/N_{p3}) The THB functions to control the power flow in the proposed HESS using a simple phase-shift modulation.

Figure 4 shows the diagram of Δ-type primary-referred equivalent circuit of the THB. The "Δ" type model is convenient for power relation analysis and the three-port model is decomposed into three two-port models. Inductances $L_{P13'}$, $L_{P3'2}$ and $L_{P2'1}$ act as energy transfer elements. Note that the symbol (') is used to denote the referred values i.e. $L_{P3'2}$ is the total inductance PHB_2 and PHB_2-referred inductance of PHB_3. The converters PHB_1, PHB_2 and PHB_3 generate square wave ac-voltages at the transformer terminal. The power flow in the proposed HESS is controlled by the phase shift angles $\emptyset_{P13}$, $\emptyset_{P12}$ and $\emptyset_{P23}$, which are the phase differences of V_{P1} and V_{P3} , V_{P1} and V_{P2} and V_{P2} and V_{P3}, respectively. Based on the figure, the power flow from port 1 to port 3, port 2 to port 1, and port 3 to port 2 are respectively determined as,

$$P_{13} = \frac{V_{BT}^2 \emptyset_{P13}(\pi - |\emptyset_{P13}|)}{\omega L_{P13'}\pi},$$
$$P_{21} = -\frac{V_{UC}^2 n_2^2 \emptyset_{P12}(\pi - |\emptyset_{P12}|)}{4D_{SB1}^2 \omega L_{P2'1}\pi},$$
$$P_{32} = -\frac{V_{HV}^2 n_3^2 \emptyset_{P23}(\pi - |\emptyset_{P23}|)}{4\omega L_{P3'2'}\pi}, \quad (1)$$

where $\emptyset$ is measured in radian, ω is the angular switching frequency, D_{SB1} is duty cycle of switching device S_{B1}.

An important feature of the multiple-input bidirectional isolated dc-dc converter is to directly supply power from one port to another port based on the virtual isolation scheme that was introduced in [14]. The basic principle is to control the phase-shift angle between three ac-voltages in order to achieve the net output power of the third port to be zero. Since the total net power of the third dc-dc converter ports is zero, the net power can be supplied from one port to other port [15].The output power of ports 1, 2 and 3, P_1, P_2, and P_3 can be calculated as,

$$P_1 = P_{13} - P_{21},$$
$$P_2 = P_{21} - P_{32},$$
$$P_3 = P_{32} - P_{13}. \quad (2)$$

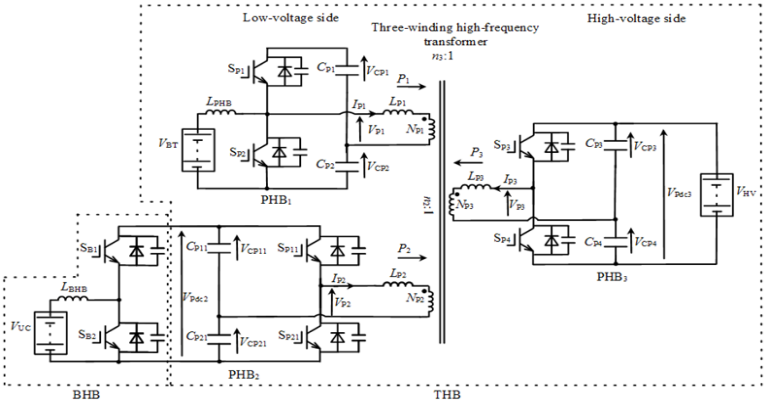

Figure 3. The proposed HESS with the rated power at: PHB_1 = 6kW, BHB and PHB_2 = 8kW, PHB_3 = 12kW.

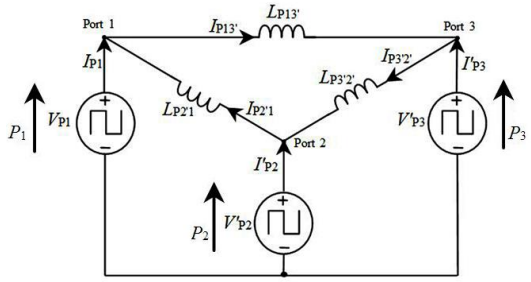

Figure 4. Δ-type primary-referred equivalent circuit of the THB.

If the loses are neglected, the total output power of the three ports is calculated as,

$$P_1 + P_2 + P_3 = 0 \quad (3)$$

The proposed HESS is analysed in 3 modes of operations. The EV motor is connected to the high-voltage bus of the proposed HESS. The power demand of the EV motor is assumed proportional to the motor rotational speed. Mode 1 (boost mode) is simulated for low power demand where power is transferred from the battery to the EV motor. Mode 2 (boost mode) is simulated for pulsed power demand where power is transferred from the battery and ultracapacitor to the EV motor. Lastly, mode 3 (buck mode) is simulated for breaking of EV where power is transferred from the EV motor to the ultracapacitor. Mode 2 is analysed in the next section. Modes 1 and 3 can be analysed in the same principle as mode 2.

2.1. Analysis of Mode 2 Operation

In mode 2, the EV motor is accelerating and the motor rotational speed is high. Therefore, the power demand of the EV motor increases rapidly. Both battery and ultracapacitor supply the power to the EV motor in order to prevent the battery output power from exceeding its rated value. At this mode, the net power between converters PHB_1 and PHB_2 is zero, where the phase-shift angle $\emptyset_{P21}$ is zero P_{21} is zero.

Figure 5 shows the idealised ac-side voltage and current, and the individual port current waveform during one switching period in mode 2. Figure 6 presents the simplified Δ-type primary-referred equivalent circuit of the THB converter that corresponds to each duration in Figure 5. The operating principles during mode 2 are presented as,

1. Duration 1($t_1 – t_2$): Switching device S_{P2} is turned off and switching device S_{P1} is turned on. The current $I_{P13'}$ flows through the anti-parallel diodes D_{P4} and D_{P1}. The stored energy in inductor $L_{P13'}$ charges the capacitors C_{P4} and C_{P1}. At the same time, switching device S_{P21} is turned off and switching device S_{P11} is turned on. The current $I_{P3'2'}$ flows through the anti-parallel diodes D_{P4} and D_{P11}. The stored energy in inductor $L_{P3'2'}$ charges the capacitors C_{P4} and C_{P11}.
2. Duration 2($t_2 – t_3$): Current $I_{P13'}$ changes its direction from negative to positive value, and flows through switching devices S_{P1} and S_{P4} and discharges capacitors C_{P1} and C_{P4}. The current $I_{P3'2'}$ changes its direction from positive to negative value, and flows through switching devices S_{P11} and S_{P4} and discharges capacitors C_{P11} and C_{P4}.
3. Duration 3($t_3 – t_4$): Switching device S_{P4} is turned off and switching device S_{P3} is turned on. The current $I_{P13'}$ flows through the switching device S_{P1} and anti-parallel diode D_{P3}. Current is transferred from battery to inductor $L_{P13'}$ and EV motor. The current $I_{P3'2'}$ flows through the switching device S_{P11} and anti-parallel diode D_{P3}. Current is transferred from ultracapacitor to inductor $L_{P3'2'}$ and EV motor.
4. Duration 4($t_4 – t_5$): Switching device S_{P1} is turned off and switching device S_{P2} is turned on. The current $I_{P13'}$ flows through the anti-parallel diodes D_{P2} and D_{P3}. The capacitors C_{P2} and C_{P3} are charged by stored in inductor $L_{P13'}$. At the same time, switching device S_{P11} is turned off and switching device S_{P21} is turned on. The current $I_{P3'2'}$ flows through the anti-parallel diodes D_{P21} and D_{P3}. The capacitors C_{P21} and C_{P3} are charged by stored in inductor $L_{P3'2'}$.
5. Duration 5($t_5 – t_6$): Current $I_{P13'}$ changes its direction from positive to negative value, and flows through switching devices S_{P3} and S_{P2} and discharges capacitors C_{P3} and C_{P2}. The current $I_{P3'2'}$ changes its direction from negative to positive value, and flows through switching devices S_{P3} and S_{P21} and discharges capacitors C_{P3} and C_{P21}.

Duration 6($t_6 – t_7$): Switching device S_{P3} is turned off and switching device S_{P4} is turned on. The current $I_{P13'}$ flows through anti-parallel diode D_{P4} and switching device S_{P2}. Current is transferred from EV motor to inductor $L_{P13'}$ and battery. The current $I_{P3'2'}$ flows through anti-parallel diode D_{P4} and switching device S_{P21}.

Its charges capacitor C_{P4} and discharges capacitor C_{P21}. Current is transferred from EV motor to inductor $L_{P3'2'}$ and ultracapacitor.

3. POWER FLOW CONTROL

The power controller manages the power transfer and aids in minimizing the device current stress even in a wide operating voltage range. When the ratio of the dc-link voltage is equal to transformer turn ratio, the transformer ac-current can be symmetrical and a so called "flat-topped" waveform can be achieved to minimize the device current stress. In the analysis of the control strategy, voltages V_{HV} and V_{BT} are assumed constant at 300 V and 100 V, respectively. The ultracapacitor voltage V_{UC} varies between 60 V and 120 V. The duty cycle of S_{B1} and S_{B2}, D_{SB1} and D_{SB2} are controlled to ensure that reference voltage V^*_{Pdc2} is constant at desired voltage of 150 V. The duty cycles of S_{B1} and S_{B2} can be described as,

$$D_{SB1} = V_{UC}/V^*_{Pdc2} \quad (3)$$

$$D_{SB2} = 1 - D_{SB1} \quad (4)$$

Figure 7 shows block diagram of the power controller for the proposed HESS. The control strategy of power transfer between the on-board energy storage device and load is based on the total load power demand. The function of power management logic block is to ensure that the power supplied from or to the battery does not exceed the battery rated power and performs the three modes of operation. The controller first identifies the required mode of operation: mode 1 and 2 (boost modes) or mode 3 (buck mode). Subsequently, it determines the power flow directions. Then, phase-shift angles $\emptyset_{P13}$ and $\emptyset_{P23}$ are calculated based on power P_{13} and P_{23} of (1).

In mode 1, the logic block assigns that power P_{21} is equal to P_{32} in order to ensure the net power of converter PHB_2 is zero (virtual isolation) and that the ultracapacitor does not supply power to the EV motor in this mode. Therefore, voltage V_{P1} leads V_{P2} and V_{P3}, in order to transfer power from converter PHB_1 to converter PHB_3. If the EV power demand during acceleration is higher than the rated power of the battery, mode 2 is performed. The logic block assigns the phase-shift angle $\emptyset_{P21}$ to be zero in order to prevent the power flow between converters PHB_1 and PHB_2. Voltages V_{P1} and V_{P2} leads V_{P3}, in order to transfer power from the converters PHB_1 and PHB_2 to converter PHB_3. In buck mode, mode 3, the logic block assigns the power P_{13} is equal to the P_{21} in order to keep converter PHB_1 in zero net power transfer. Therefore, the battery is not charged and is in virtual isolation, and all the regenerative braking power charges the ultracapacitor at this mode. Voltage V_{P3} leads V_{P1} and V_{P2} in order to transfer power from converter PHB_3 to converter PHB_2.

4. POWER DEMAND OF THE HESS FROM AN EV

The proposed HESS is verified through simulations using the PSCAD software. Several assumptions are made to simplify the analysis of the operation. The HESS supplies power to the EV motor at a constant voltage. The EV motor power demand is assumed to be proportional to the speed of rotation of the dc motor at a constant load torque. Figure 8 present the idealized battery, ultracapcitor, and EV motor power requirement for various modes of operations such as constant speed, acceleration and deceleration.

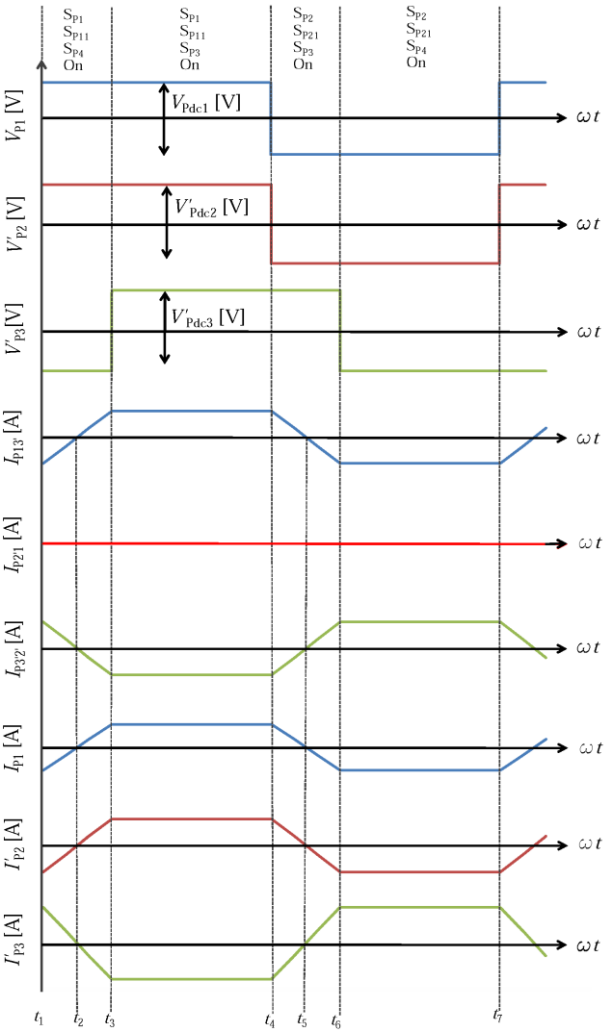

Figure 5. Idealised ac-side voltage and current waveforms, and current waveforms of each port during a steady-state in mode-2 operation.

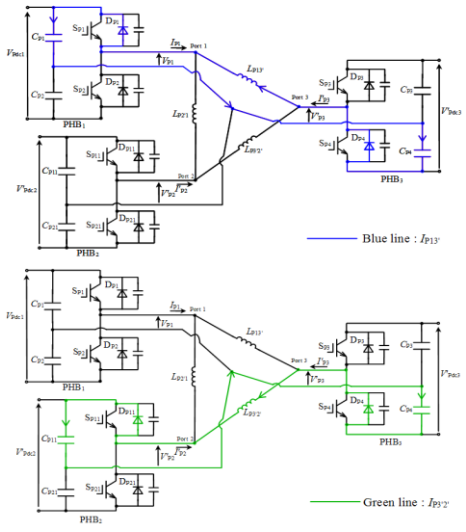

(a)

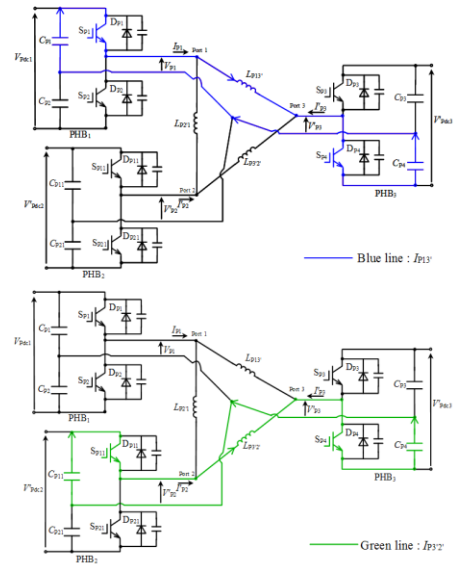

(b)

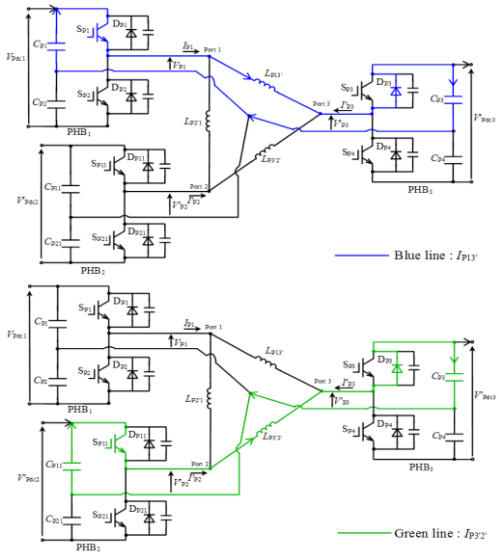

(c)

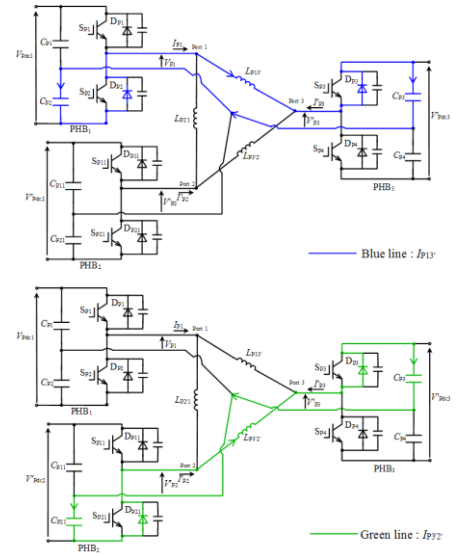

(d)

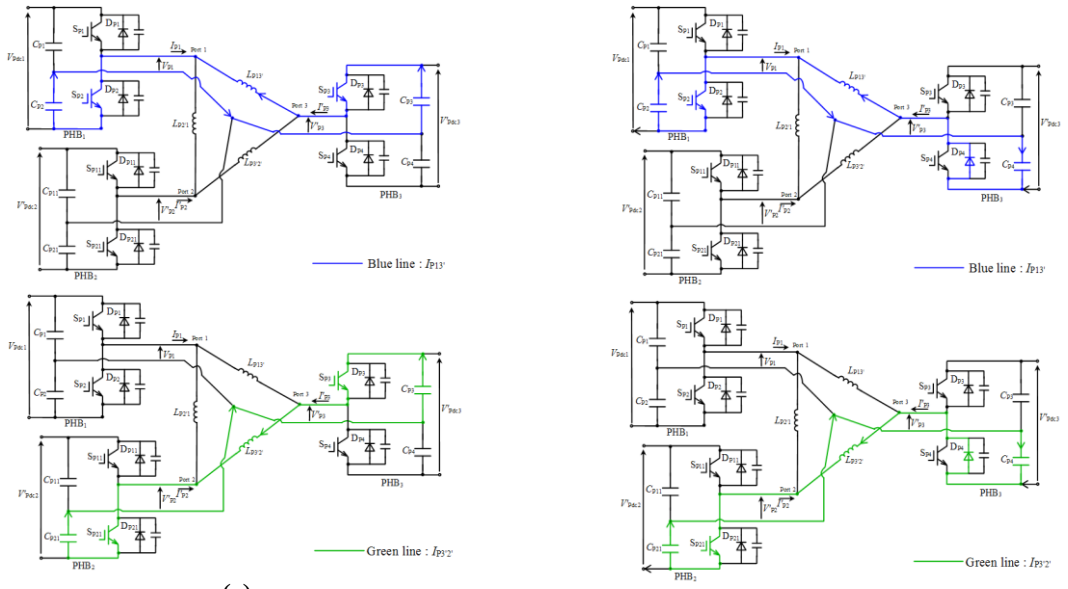

(e) (f)

Figure 6. Equivalent circuit during a switching cycle in mode 2, corresponding to Figure 5. (a) Duration 1 (t_1 - t_2). (b) Duration 2 (t_2 - t_3). (c) Duration 3 (t_3 - t_4). (d) Duration 4 (t_4 - t_5). (e) Duration 5 (t_5 - t_6). (f) Duration 6 (t_6 - t_7).

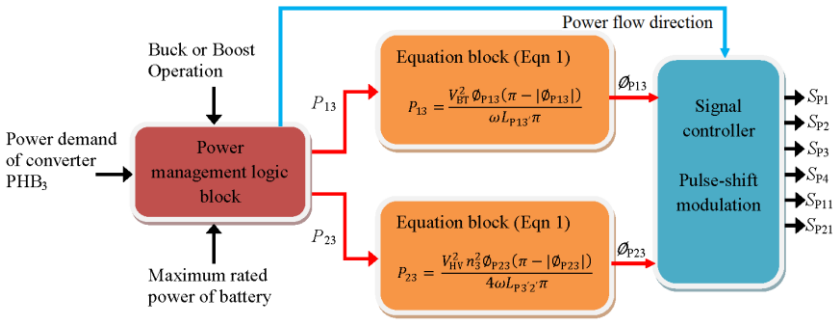

Figure 7. Power controller of the proposed HESS.

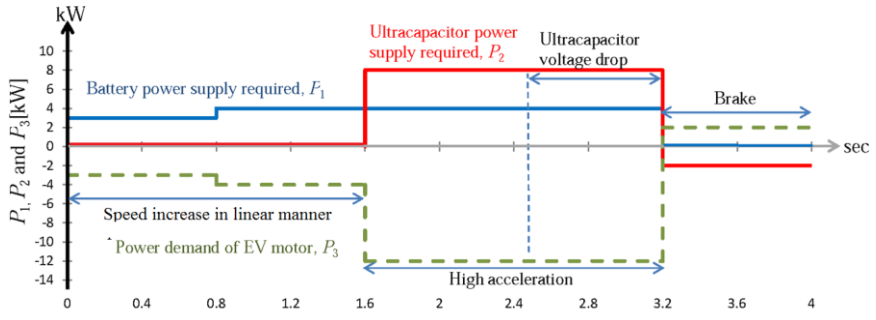

Figure 8. Idealized battery, ultracapacitor, and EV motor power during the various modes of operation as calculated by the power management logic block in Figure 7.

5. SIMULATION RESULTS

In the simulation, the battery voltage V_{BT} and high-side voltage V_{HV} are constant at 100V and 300V, respectively. The voltage of ultracapacitor, V_{UV}, varies between 60 V to 120 V. The duty cycle of THB switching devices (D_{SP1}–D_{SP4}, D_{SP11}–D_{SP21}) are constant at 0.5 p.u. The duty cycle of the BHB switching

device D_{SB1} and D_{SB2} is between 0.2 and 0.8 p.u. Table 1 presents the circuit parameters of the capacitive and magnetic components of the THB converter.

Table 1. THB Circuit Parameters

Transformer turns ratio	$N_{P1} : N_{P2} : N_{P3}$	100:150:300
AC inductor of PHB_1	L_{P1}	4.41 µH
AC inductor of PHB_2	L_{P2}	1.24 µH
AC inductor of PHB_3	L_{P3}	1.37 µH
Capacitors of PHB_1	C_{P1} and C_{P2}	0.5 mF
Capacitors of PHB_2 and PHB_3	C_{P11}, C_{P21}, C_{P3},C_{P4}	1 mF
Snubber capacitor of THB		10 nF
DC-link inductor of PHB_1	L_{PHB}	833 µH
DC-link inductor of BHB	L_{BHB}	360 µH
Switching frequency		20 kHz

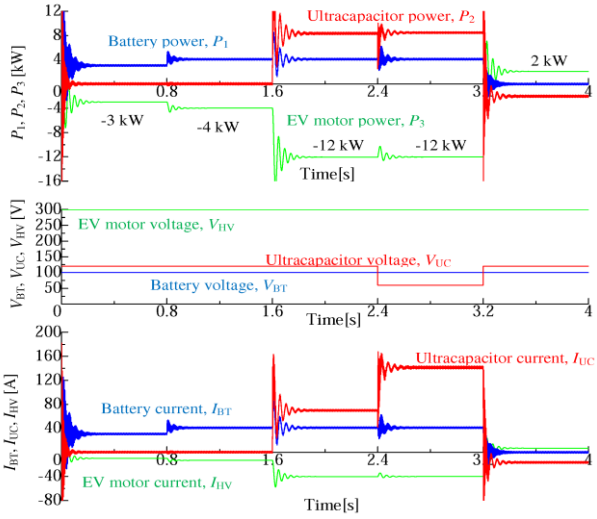

Figure 9. Simulation results of the power, dc voltage, and dc current waveforms of battery, ultracapacitor and EV motor during all modes of operation.

Figure 9 shows the simulation results of EV motor, battery, and ultracapacitor power for the duration of 4s. The battery power P_1 is determined from the product of V_{BT} and I_{BT}. The ultracapacitor power P_2 and EV motor power P_3 are determined from the product of V_{UC} and I_{UC}, and voltage V_{HV} and I_{HV}, respectively. Both the battery and ultracapacitor are able to supply the power variation required by the EV motor, while keeping the battery power below the rated power. This verifies the feasibility of the power management unit in controlling the phase-shift angle to split the output power between the battery and ultracapacitor. Moreover, the converter PHB_2 is able to supply constant power when ultracapacitor voltage V_{UC} drops from 120 V to 60V during simulation time of 2.4s to 3.2s. During the simulation time from 3.2s to 4s, the ultracapacitor power changes from positive to negative, showing that the dc current direction of the converter is reversed and the ultracapacitor is charged.

Figure 10 shows the ac-side voltage and current waveforms of convertors PHB_1, PHB_2 and PHB_3 of mode 1, battery discharging. The phase-shift angles $\emptyset_{P13}$ and $\emptyset_{P23}$ are 15.73° and 1.81°, respectively. Based on the power flow calculation in (1), $P_{21} = P_{32}$. Therefore, the ultracapacitor power P_2 is zero (virtual isolation) and battery power P_1 is 4 kW. Current i_2 is approximately zero, verifying that converter PHB_2 has zero net power transfer between 0.8s to 1.6s. The ac current are seen to be having low rate of change of current during the conduction period.

Figure 11 presents the ac-side voltage and current waveforms of convertors PHB_1, PHB_2 and PHB_3 and ultracapacitor current during steady state operation of mode 2. The power management logic block assigns converter PHB_2 to supply power in achieving power demand of EV motor. The phase-shift angles $\emptyset_{P13}$ and $\emptyset_{P23}$ are 20.21° and 20.21°, respectively. Currents I_{P1}, I_{P2}, and I_{P3} are not zero verifying that converters PHB_1, PHB_2, and PHB_3 have power flow. When V_{UC} reduces its voltage to 60V between 2.4s and 3.2s, it is observed that the ratio of peak voltage of V_{P1}, V_{P2} and V_{P3} is equal to the transformer turn ratio, and

current I_{P2} remains symmetrical and has a "flat top". This verifies that the control of duty cycles D_{SB1} and D_{SB2} are able to ensure voltage V_{Pdc2} is constant at 150 V, minimizing the device current stress. The current I_{UC} increases when the voltage V_{UC} reduces. The ultracapacitor supply higher current I_{UC} to maintain a constant power supply of 8 kW.

Figure 12 shows the ac-side voltage and current waveforms of convertors PHB_1, PHB_2 and PHB_3 in mode 3, regenerative breaking. The phase-shift angles $\emptyset_{31}$ and $\emptyset_{32}$ are 0.93° and 4.12°, respectively. Based on the power flow calculation in (1), the battery power is zero (virtual isolation) and ultracapacitor power is −2 kW. The current I_{P1} of converter PHB_1 is approximately zero. It verifies that converter PHB_1 is in zero net power transfer and that battery is not charged during regenerative braking power.

The results in this section show that the proposed HESS and its power management for EV application achieves the desired power flow with minimal current stress at PHB_2 as the ultracapacitor voltage changes from 1 p.u. to 0.5 p.u. of the rated voltage. The proposed topology needs only simple phase-shift modulation. The power management controller also shows good dynamic response to step changes in power demand and ultracapacitor voltage.

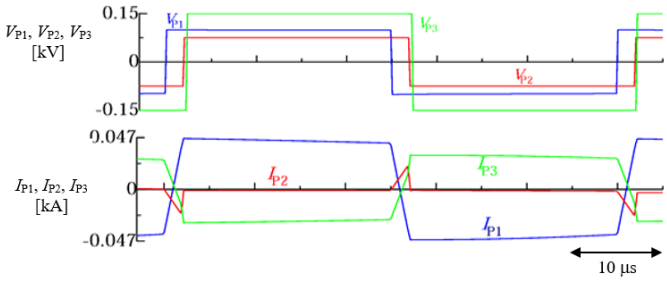

Figure 10. Enlarged steady-state AC voltage and current waveforms of convertors PHB_1, PHB_2 and PHB_3 in mode 1 that occurred between t=0.8s and t=1.6s of Figure 8.

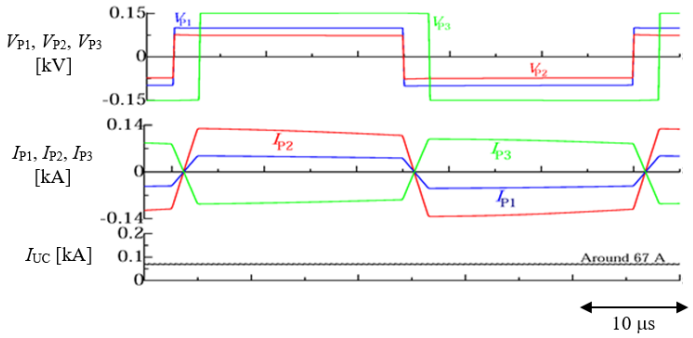

(a)

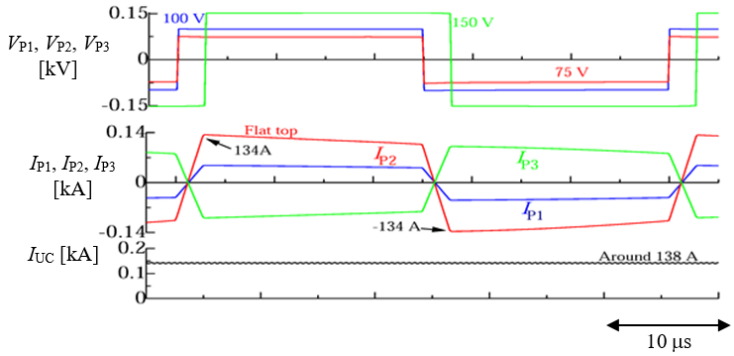

(b)

Figure 11. Enlarged steady-state AC voltage and current waveforms of convertors PHB_1, PHB_2 and PHB_3 in mode 2 that occurred between t=1.6s and t=3.2s of Figure 8. (a)V_{UC}=120V. (b) V_{UC}=60V

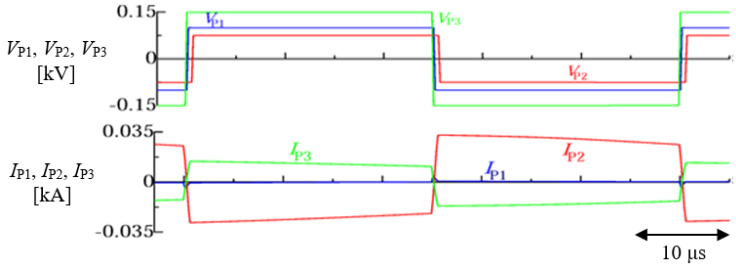

Figure 12. Enlarged steady-state AC voltage and current waveforms of convertors PHB_1, PHB_2 and PHB_3 in mode 3 that occurred between t=3.2s and t=4s of Figure 8.

6. CONCLUSION

The proposed HESS has been designed so that battery and ultracapacitor energy storage devices are able to supply the maximum power demand during acceleration of an EV. Moreover, the ultracapacitor can rapidly absorb the regenerative power from braking of motor to ensure that the battery charge-discharge cycle is minimized, thus extending the lifetime of the battery. The advantages of the proposed HESS include galvanic isolation, fewer components compared to full-bridge topologies, and simple phase-shift modulation. In order to facilitate the understanding of the operating principles of the proposed HESS, detail discussions on the ideal operating waveforms and analysis of the switching equivalents circuits have also been presented. Simulation results using PSCAD show the feasibility of the power management controller in all operating conditions with good dynamic response and minimized device current stress.

ACKNOWLEDGEMENTS

The authors would like to thank the Ministry of Higher Education and Universiti Tenaga Nasional for providing financial support through FRGS Project No. FRGS/1/2017/TK04/UNITEN/02/4 and BOLD Grant Project No. 10289176/B/9/2017/48.

REFERENCES

[1] R. Spotnitz, "Advanced EV and HEV batteries," Proc. *IEEE Conf. Vehicle Power and Propulsion,* Sept. 2005, pp. 334-337.
[2] J. M. Miller, T. Bohn, T. J. Dougherty, and U. Deshpande, "Why hybridization of energy storage is essential for future hybrid, plug-in and battery electric vehicles," Proc. *IEEE Energy Conversion Congress and Exposition (ECCE),* Sept. 2009, pp. 2614-2620.
[3] Z Zhu and B. Yang, "The research on intelligent management system of li-ion power battery string of electric vehicle," Proc. *Int. Conf. Electronics, Communications and Control (ICECC),* Sept. 2011, pp. 2370-2372.
[4] A. Lavanya, K. V. Kumar, J. D. Navamani, "Topological Comparison of Dual-Input DC-DC Converters," *International Journal of Power Electronics and Drive System (IJPEDS),* vol. 8, no. 2, pp. 804 – 811, June 2017.
[5] T. K. Santhosh and C. Govindaraju, "Development of Predictive Current Controller for Multi-Port DC/DC Converter," *International Journal of Power Electronics and Drive System (IJPEDS),* vol. 6, no. 4, pp. 683 – 692, Dec. 2015.
[6] F. Z. Peng, H. Li, G-J. Su, and J. S. Lawler, "A new ZVS bidirectional dc-dc converter for fuel cell and battery application," *IEEE Trans. Power Electron.*, vol. 19, no. 1, pp. 54-65, Jan. 2004.
[7] Z. Li, O. Onar, A. Khaligh, and E. Schaltz, "Design and control of a multiple input dc/dc converter for battery/ultracapacitor based electric vehicle power system," *Proc. Applied Power Electronics Conference and Exposition (APEC),* Feb. 2009, pp. 591-596.
[8] S. Cui, D. He, M. Li, H. Lu, and T. G. Habetler, "Design of a dual half bridge DC-DC converter for an ultra-capacitor based auxiliary power source in electric vehicles," Proc. *IEEE Transportation Electrification Conference and Expo (ITEC),* June 2012, pp. 1-7.
[9] H. Li and F. Z. Peng, "Modeling of a new ZVS bi-directional dc-dc converter," *IEEE Trans. Aerospace and Electronic Systems,* vol. 40, no. 1, pp. 272-283, Aug. 2004.
[10] S. Han and D. Divan, "Bi-directional DC/DC converters for plug-in hybrid electric vehicle (PHEV) applications," Proc. *IEEE Applied Power Electronics Conference and Exposition (APEC),* Feb. 2008, pp. 784-789.
[11] D. Xu, C. Zhao, and H. Fan, "A PWM plus phase-shift control bidirectional DC-DC converter," *IEEE Trans. Power Electron.*, vol. 19, no. 3, pp. 666-675, May 2004.
[12] S. Cui, D. He, Z. Chen, and T.G. Habetler, "A wide input voltage range ZVS isolated bidirectional DC-DC converter for ultra-capacitor application in hybrid and electric vehicles," *Proc. IEEE Conf. Electric Vehicle (IEVC),* Mar. 2012, pp. 1-6.

[13] H. Tao, J. L. Duarte, and M. M. Hendrix, "Three-port triple-half-bridge bidirectional converter with zero-voltage switching," *IEEE Trans. Power Electron.*, vol. 23, no. 2, pp. 782-792, Mar. 2008.
[14] S-Y. Kim, H-S. Song, and K. Nam, "Idling port isolation control of three-port bidirectional converter for EVs," *IEEE Trans. Power Electron.*, vol. 27, no. 5, pp. 2495-2506, May 2012.
[15] C. Zhao, S.D. Round, and J. W. Kolar, "An isolated three-port bidirectional dc-dc converter with decoupled power flow management," *IEEE Trans. Power Electron.*, vol. 23, no. 5, pp. 2443-2453, Sept. 2008.

BIOGRAPHIES OF AUTHORS

Tan Boon Kai received the B. Eng. (Hons) degree in Electrical and Electronic Engineering from UCSI University, Kuala Lumpur, Malaysia in 2012 and the M. Eng. Degree in Electrical Engineering from Universiti Tenaga Nasional, Kajang, Malaysia in 2014. His main research interests are in areas of plug-in electric vehicles. He is currently working for Squire Mech Sdn. Bhd. Malaysia.

Nadia Tan Mei Lin received the B.Eng. (Hons.) degree from the University of Sheffield, Sheffield, U.K., in 2002, the M. Eng. degree from Universiti Tenaga Nasional, Kajang, Malaysia, in 2007, and the Ph.D. degree from Tokyo Institute of Technology, Tokyo, Japan, in 2010, all in electrical engineering. Since April 2017, she has been an Associate Professor in the Department of Electrical Power Engineering, Universiti Tenaga Nasional. Her current research interests include power conversion systems for energy storage, bidirectional isolated dc–dc converters, multilevel cascaded inverters for renewable energy applications. She is a Chartered Engineer registered with Engineering Council, United Kingdom, a Member of the Institution of Engineering and Technology (IET) and the Institute of Electrical and Electronics Engineers (IEEE), and a Graduate Member of the Institution of Engineers Malaysia (IEM).

Agileswari K. Ramasamy was born in Taiping, Perak and received her B.Sc (Engineering) degree from Purdue University, USA in 1995 under the sponsorship of Yayasan Tenaga Nasional. She obtained her MSc. (Control System) from Imperial College, London in 2001 and PhD in Electrical Engineering from Universiti Tenaga Nasional (UNITEN), under the sponsorship of UNITEN. She is currently an Associate Professor in the Department of Electronics Communication Engineering at UNITEN and serving as a Deputy Dean of Research and Postgraduate for College of Engineering, UNITEN. She is also a Chartered Member of the Institution of Engineering and Technology (IET). She is currently active in research and consultancy in control system, power system, power quality, energy efficiency and renewable energy. She has headed several research projects to date and has successfully published several indexed journals.